Full length article

Lateral–torsional buckling resistance of corrugated web girders based on deterministic and stochastic nonlinear analysis

E. Bärnkopf, B. Jáger *, B. Kövesdi

Budapest University of Technology and Economics, Faculty of Civil Engineering, Department of Structural Engineering, H-1111 Budapest, Műegyetem rkp. 3., Hungary

ARTICLE INFO

ABSTRACT

There is no commonly accepted and reliable design method to determine the lateral–torsional buckling (LTB) resistance of steel trapezoidally corrugated web girders. Therefore, the focus of the current paper is on the investigation of this failure mode, detailed evaluation of the structural behavior and determination of the accurate LTB resistance. An advanced finite element (FE) model is developed and validated using the results of laboratory test performed at the Budapest University of Technology and Economics in 2018. Based on the experimental background virtual tests are performed on a simply supported beam subjected by pure bending moment. The effect of the different flange sizes, corrugation layouts, boundary conditions and steel grade including high-strength steel as well, are investigated. Two kinds of parametric studies are performed using (i) deterministic and (ii) stochastic nonlinear analysis. In both cases the imperfections have a key role in the FEM-based resistance calculation. Therefore, the imperfections are considered as initial geometric imperfections and residual stress, and also as equivalent geometric imperfections and their results are compared. The required equivalent geometric imperfection magnitude is determined and proposed in such a way to achieve the same impact as the initial geometric imperfection and residual stresses have. By both the deterministic and stochastic analysis results the required buckling curve of the Eurocode is determined by reliability assessment. The results of the two different analyses are compared and design recommendation is given for reduction factor determination for trapezoidally corrugated web girders.

1. Introduction

Reducing the material consumption of the structures parallel with their sensitivity to web buckling and simplifying their transport and installation have motivated the development of trapezoidally corrugated web girders. These girders are modifications of traditional I-beams by using a corrugated web instead of flat webs. In the case of bridge girders with conventional flat webs transverse and longitudinal stiffeners are subsequently welded to the web panels to eliminate the sensitivity to web buckling; this process needs a great amount of labor work. An alternative to this is the application of corrugated web girders in which no stiffeners are needed to be added for strengthening and the web panel can be thinner than in those of conventional girders. This generally allows to build lighter structures and avoids the need for post-welding, however, it requires special technology for the manufacturing of trapezoidally corrugated web girders.

Trapezoidally corrugated web girders are increasingly used in the structural engineering practice due to their numerous favorable properties. The structural behavior of these girders is different from that of girders with flat webs therefore they require detailed investigations.

Many open questions are still unanswered about the lateral–torsional buckling (LTB) behavior of corrugated web girders, which is the topic of the current paper. Many research programs carried out so far focusing on the determination of the elastic critical moment and there is no generally accepted method for the determination of the lateral–torsional buckling resistance. Therefore, the aims of the current study are (i) to determine the required equivalent geometric imperfection shape and magnitude being applicable for geometrical and material nonlinear imperfect analysis (GMNIA) connected to the manufacturing tolerances of the EN 1090 [1] standard and (ii) to determine which of the lateral–torsional buckling or flexural buckling curves of EN1993-1-1 [2] can be used for the determination of the LTB resistance of trapezoidally corrugated web girders. In addition, the effect of different corrugation web arrangements, boundary conditions and steel grades are investigated. The required buckling curves are determined in two ways, first a deterministic numerical analysis then stochastic analysis is carried out. In the stochastic analysis, geometrical and material properties are determined as probabilistic variables and Monte Carlo simulations (supplemented by the response surface method) are executed to determine the mean and the characteristic values of the LTB
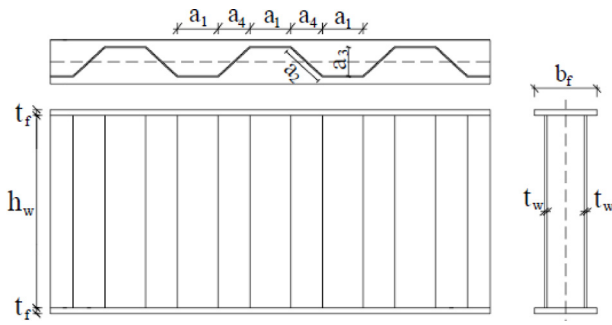
Fig. 1. Applied notations.

resistance for typical and representative cross-sections. Based on the results of the deterministic and stochastic analyses, semi-probabilistic reliability assessment methodologies are applied to define the safety level of the buckling curves of the EN 1993-1-1 [2] (level #1.). In the stochastic calculation the so-called first-order reliability analysis (FORM) is used (level #2.) according to EN 1990 [3], which already takes into account the uncertainty in the evaluation of the structure due to the geometric and material properties. The applied notations used in the paper are given in Fig. 1.

2. Literature review

2.1. Elastic critical moment

The first studies were carried out by Lindner [4] who showed the elastic critical moment of trapezoidally corrugated web girders, and their lateral–torsional buckling resistance is greater than that of girders having conventional flat web. After that numerous researchers, among others Sayed-Ahmed [5], Moon et al. [6], Nguyen et al. [7], Zhang et al. [8], Larsson and Persson [9] and Ilanovsky [10] confirmed this statement. The elastic critical moment for flat web girder subjected to uniform bending moment can be calculated by Eq. (1) according to Timoshenko and Gere [11].

$$M_{cr} = \frac{\pi}{k \cdot L} \sqrt{E I_Z \left[\left(\frac{\pi}{k_w \cdot L} \right)^2 E I_w + G I_t \right]} \tag{1}$$

In the above equation E is the elastic modulus, G is the shear modulus, L is the span length, Iz is the moment of inertia about the minor axis, It is the torsional constant, Iw is the warping constant, k is the effective length factor about the weak axis rotation and kw is the effective length factor with respect to warping.

Lindner [4] modified the above formula for trapezoidally corrugated web girders introducing an additional term with a correction factor c_w in the warping constant given by Eq. (2) in order to consider the greater performance. Conspicuous, this additional term includes the length, despite of the fact that the warping constant is a sectional property. According to Lindner the factors u_x and c_w should be calculated by Eqs. (3)–(4), and then Eq. (1) can be applied for corrugated web girders as well by substituting the increased warping constant.

$$I_w = I_{w,flat} + c_w \frac{L^2}{E \pi^2} \tag{2}$$

$$c_w = \frac{a_3^2 \cdot (h_w + t_f)^2}{c_1 \cdot u_x \cdot (a_1 + a_4)} \tag{3}$$

$$u_x = \frac{(h_w + t_f)}{2 \cdot G \cdot a_1 \cdot t_w} + \frac{(h_w + t_f)^2 \cdot (a_1 + a_4)^3}{c_2 \cdot a_1^2 \cdot E \cdot b_f \cdot t_f^3} \tag{4}$$

In the above equations $I_{w,flat}$ is the warping constant of flat web girders, $c_1 = 8$ and $c_2 = 25$ are constants according to Lindner. Moon et al. [6], Nguyen et al. [7], Zhang et al. [8] and Ibrahim [12] also proposed different methods to consider the increase of the elastic critical moment.

Table 1
The imperfection factor for different buckling curves.

	a_0	a	b	c	d
α_{LT}	0.13	0.21	0.34	0.49	0.79

Larsson and Persson [9] made a comprehensive numerical study in 2013 and confirmed the formula proposed by Lindner. In this research Larsson and Persson rearranged the formula by assigning the additional term to the torsional constant according to Eq. (5). The two versions give the same result, but with this modification none of the sectional properties are dependent on the length of the girder.

$$I_t = I_{t,flat} + \frac{c_w}{G} \tag{5}$$

In this formula c_w remains the correction factor for trapezoidally corrugated web girders introduced by Lindner. Using the suggestion of Larsson and Persson, Lopes et al. in their research [13] investigated sinusoidally and trapezoidally corrugated web girders and based on an extensive numerical study they modified the parameters to $c_1 = 22$ and $c_2 = 300$. Guo and Papangelis [14] investigated and compared girders with trapezoidally corrugated and flat web. They applied torsional moments to the beams and found that the torsional constant is significantly higher for trapezoidally corrugated web girders, however, there is just a minor difference between the warping constants. This also confirmed the validity of Larsson and Persson's interpretation. Other proposals have been also made to address this issue. Sayed-Ahmed [5] suggested an equivalent web thickness; Moon et al. [6], Nguyen et al. [7], Kazemi [15] and Ibrahim [12] considered the effect of the trapezoidally corrugated web by reducing the shear modulus; and Ilanovsky [10] provided a simple multiplication factor to modify the elastic critical moment for flat web girders.

2.2. Lateral–torsional buckling resistance

According to EN1993-1-1 [2] the reduction factor (χ_{LT}) for the lateral–torsional buckling strength for rolled sections or equivalent welded sections with flat web may be calculated by Eqs. (6)–(8).

$$\chi_{LT} = \frac{1}{\Phi_{LT} + \sqrt{\Phi_{LT}^2 - \beta \bar{\lambda}_{LT}^2}} \text{ but } \chi_{LT} \leq \min \left(1.0; \frac{1}{\bar{\lambda}_{LT}^2} \right) \tag{6}$$

$$\Phi_{LT} = \frac{1 + \alpha_{LT} \cdot \left(\bar{\lambda}_{LT} - \bar{\lambda}_{LT,0} \right) + \beta \bar{\lambda}_{LT}^2}{2} \tag{7}$$

$$\bar{\lambda}_{LT} = \sqrt{\frac{M_y}{M_{cr}}} \tag{8}$$

In the above equations α_{LT} is the imperfection factor (the value for different buckling curves is given in Table 1), $\bar{\lambda}_{LT}$ is the relative slenderness, β is the multiplication factor and, $\bar{\lambda}_{LT,0}$ is the relative slenderness limit. In Eq. (8) M_y is the cross-sectional bending moment resistance as given by Eq. (9) where $b_{f,eff}$ is the effective width.

$$M_y = b_{f,eff} \cdot t_f \cdot f_{yf} \cdot (h_w + t_f) \tag{9}$$

Not many laboratory experiments on corrugated web girders have been carried out so far, mostly numerical studies are available in the international literature in this topic. FE analyses have been carried out by Moon et al. [6,16] and they concluded that the use of buckling curve b ($\beta = 1.0$ and $\bar{\lambda}_{LT,0} = 0.2$) of EN1993-1-1 results in conservative solutions for trapezoidally corrugated web girders. Ibrahim [12] performed advanced FE analysis on trapezoidally corrugated web girders with unequal flanges and found that the lateral–torsional buckling curve d of EN1993-1-1 is applicable using $\beta = 0.75$ and $\bar{\lambda}_{LT,0} = 0.4$; this is also confirmed by Hassanein et al. [17] who numerically studied high-strength steel girders having unequal flanges. Elkawas et al. [18] also
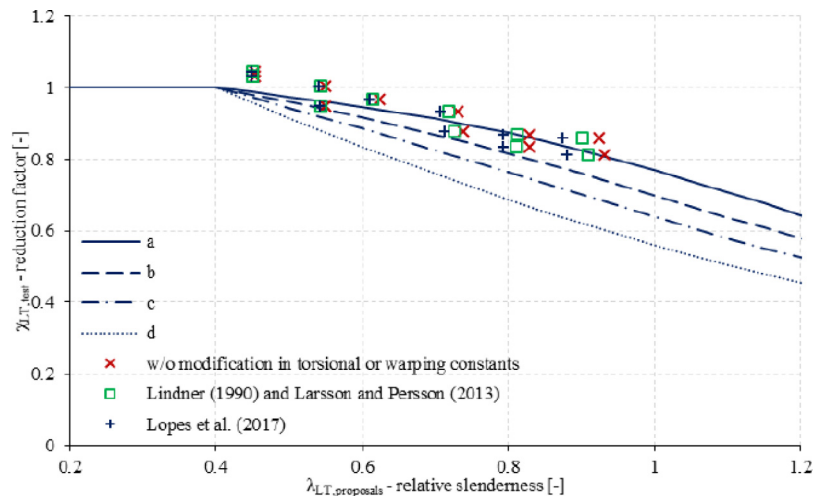
Fig. 2. Comparison of the test results and previous proposals with EN1993-1-1 lateral–torsional buckling curves [2,26].

numerically studied high-strength steel trapezoidally corrugated web girders and found that the lateral–torsional buckling curve a could be applicable using $\beta = 0.75$ and $\overline{\lambda}_{LT,0} = 0.4$. This is confirmed by Shao et al. [19] who numerically investigated the LTB strength of high-strength steel girders. According to their latest result [20] the buckling curve a_0 may be applicable for corrugated web girders.

Some experimental studies have been also performed by different researchers. Kubo and Watanabe [21] investigated nine trapezoidally corrugated web girders loaded by three-point-bending, Hannebauer [22] and Pimenta et al. [23] investigated three and four sinusoidally corrugated web girders, respectively. In addition, Zhang et al. [24] tested four sinusoidally corrugated web girders using a cantilever arrangement with concentrated load introduction at the end of the cantilever. In the Structural Laboratory of the Budapest University of Technology and Economics Department of Structural Engineering an extensive experimental research program was performed in 2018 [25]. In the frame of the experimental program eleven large-scale test specimens were investigated by four-point-bending. Six different girder geometries having different flange sizes and the same corrugation profile were examined. The test specimens were all 8.2 m long. Each specimen was loaded by pure in-plane bending and the length between the out-of-plane supports was 6000 mm in each case with limited warping and rotational restraint at the supports. The primary aim was to determine the lateral–torsional buckling resistance of the test girders. The reduction factors ($\chi_{LT,test}$) were determined from the test results and compared to the lateral–torsional buckling curves of the EN 1993-1-1 ($\beta = 0.75$ and $\lambda_{LT,0} = 0.4$) shown in Fig. 2. For the calculation of the relative slenderness ($\lambda_{LT,proposals}$) three different analytical proposals for the elastic critical moment were applied: (i) without any modification in the torsional or warping constants, (ii) with an additional term in the torsional constant proposed by Larsson and Persson presented by Eq. (5) using the constants of Lindner ($c_1 = 8$ and $c_2 = 25$) and (iii) with the constants of Lopes et al. ($c_1 = 22$ and $c_2 = 300$). Based on the results the lateral–torsional buckling curve b of EN1993-1-1 was proposed as lower bound estimate (k and k_w were set to 0.5) for the prediction of the lateral–torsional buckling resistance of trapezoidally corrugated web girders together with the elastic critical moment of Lopes et al. [13].

Jáger and Dunai [27] carried out nonlinear analyses to determine the required equivalent geometric imperfection shape and magnitude for the determination of the LTB strength of corrugated web girders. They used experimental test results as the basis of the FEM based design resistance calibration.

3. Numerical model development

3.1. Geometric model, boundary conditions and validation

Based on the laboratory experiments an advanced numerical model is developed using the finite element software Ansys 19.2 [28]. The model is verified by checking the appropriateness of the mathematical and geometrical finitizations and validated by test results. Results of the model development and validation is detailed in [27]. The numerical model used in the present paper represents a simply supported beam subjected by concentrated bending moments at both ends where the rotation about the vertical axis and warping can be fixed or free (see Eq. (1)). By these three different boundary conditions can be achieved: (i) warping and rotation free ($k_w = k = 1.0$), (ii) warping fixed and rotation free ($k_w = 0.5$ and $k = 1.0$ indicating the presence of strong transverse stiffeners at both ends), and (iii) warping and rotation fixed ($k_w = k = 0.5$). These arrangements are achieved by joining the end cross-section nodes to one master node and by assigning the corresponding degrees of freedoms to each coupling. The master node is located in the center of gravity of the end cross-sections where the vertical and lateral displacements and the twist about the longitudinal axis are constrained. The developed model is a full shell model using four-node thin shell elements (Shell 181) as shown in Fig. 3 with the finite element mesh, and boundary and loading conditions. The end moments are introduced by force couples acting on the upper and lower flanges. The required mesh size obtained in the model verification is $a_1/4$, since the mesh size is calculated as the function of the profile parameter a_1 (Fig. 1), so $a_1/4$ would be appropriate, but due to the accurate modeling of the residual stress pattern, a denser mesh is used ($a_1/8$) in the numerical parametric study.

3.2. Material model

For the nonlinear calculations a multilinear material model is used according to Gardner at al. [29] in case of normal strength steel (NSS); shown in Fig. 4. This multilinear material model can be defined from three basic parameters — elastic modulus (E), yield strength (f_y), and tensile strength (f_u). In the deterministic analysis only S355 steel grade is used with steel yield strength of $f_y = 355$ MPa, tensile strength of $f_u = 510$ MPa and elastic modulus of $E = 210$ GPa. In the stochastic analysis high strength steel material is also applied. The effect of the application of different steel grades is presented in Section 5.3.
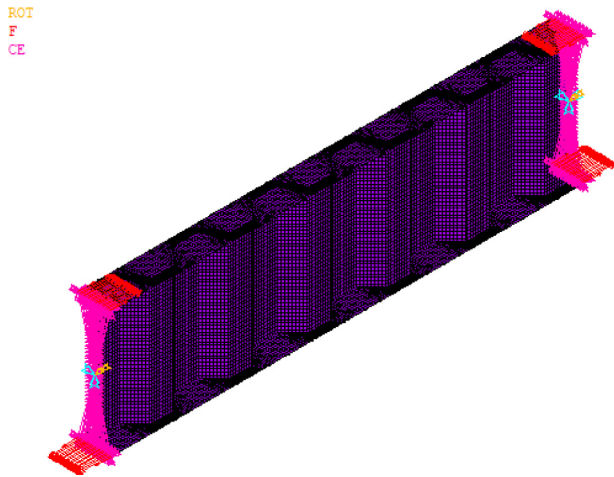
Fig. 3. Finite element model (mesh, boundary and loading conditions).
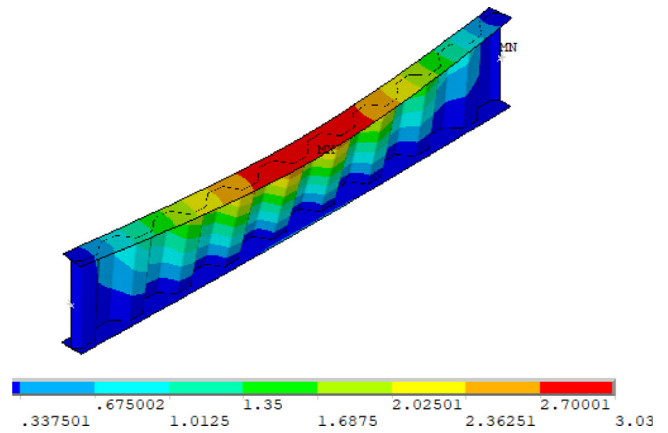

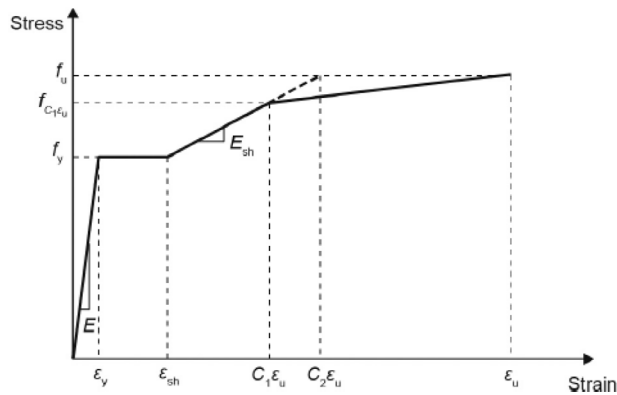Fig. 5. Applied imperfection shape.

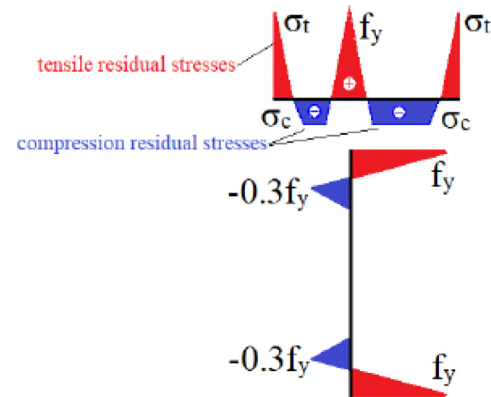Fig. 4. Multilinear material model according to Gardner et al. [29].

Fig. 6. The applied residual-stress model [27].

3.3. Geometrical imperfection — out-of-straightness

In the case of trapezoidally corrugated web girders, the standards currently do not provide global geometric imperfections, so this issue requires more careful consideration. Based on previous laboratory experiments of the authors [26], the best fit and safe side equivalent geometric imperfection magnitudes are obtained to $L/1000$ and $L/750$, respectively [27] using the first global eigenmode shape. The numerical calculations for the twelve specimens, however, show significant differences. In the current study the equivalent geometric imperfection is determined by having the same impact as the combination of the initial out-of-straightness with magnitude of $L/1000$ (manufacturing tolerance $L/1000$ in Annex B of EN 1090-2:2018 [1]) and the residual stresses have. This method gives a lower bound estimate for the LTB resistance. The results of this imperfection-sensitivity study is presented in Section 4. In addition, during the nonlinear analysis in Sections 6 and 7 both the residual stresses and initial out-of-straightness are considered rather than the equivalent geometric imperfection. In this study the first global eigenmode shape is applied as artificial geometric imperfections shown in Fig. 5.

3.4. Residual stresses

The applied residual-stress pattern is shown in Fig. 6 according to [27]. The tensile stress in the flanges is equal to the yield strength at the web-to-flange junction (f_y), and there is also tensile stress at the edges of the flange from flame-cutting. The compressive stresses in the flanges come from welding. The effect of the residual stresses in the web is much smaller, and could be negligible, due to the so called "accordion effect" (the web does not work against normal directional loads) [30,31]. There is just a small area effected by tensile residual stresses at the web-to-flange connection, followed by a small section of compressive stresses, and the large part of the web is practically free of residual stresses due to the accordion effect.

4. Required equivalent geometric imperfection

The advanced analysis requires equivalent geometric imperfection rather than the separate consideration of initial geometric imperfection and residual stress, because it is easier to apply in the FEM based design approach. Five different cross-sections are studied for imperfection-sensitivity, differing in their flange sizes and corrugation profile. In all cases the web height of the girders is 520 mm, and the web thickness is 6 mm. The cross-sections are doubly symmetrical; the five types of flanges are 140-14, 160-14, 180-14, 220-16 and 250-16 (flange width–flange thickness given in mm). The same trapezoidal corrugation profile is investigated for the different cross-sections with the parameters: $\alpha = 45°$, $a_1 = a_2 = 98$ mm; the notations are given in Fig. 1. However, for the 140-14 girders two more different corrugation angles are also studied: 30° and 40° (without changing the other parameters). In overall 6-8 different slenderness are investigated by applying different span lengths. In the imperfection-sensitivity study the scaled-up first global buckling eigenmode is applied from linear buckling analysis (LBA) as artificial geometric imperfection. The required equivalent geometric imperfection is determined in such a way to have the same impact on the FEM-based resistance as the initial geometric imperfection with magnitude of L/1000 combined with the residual stresses
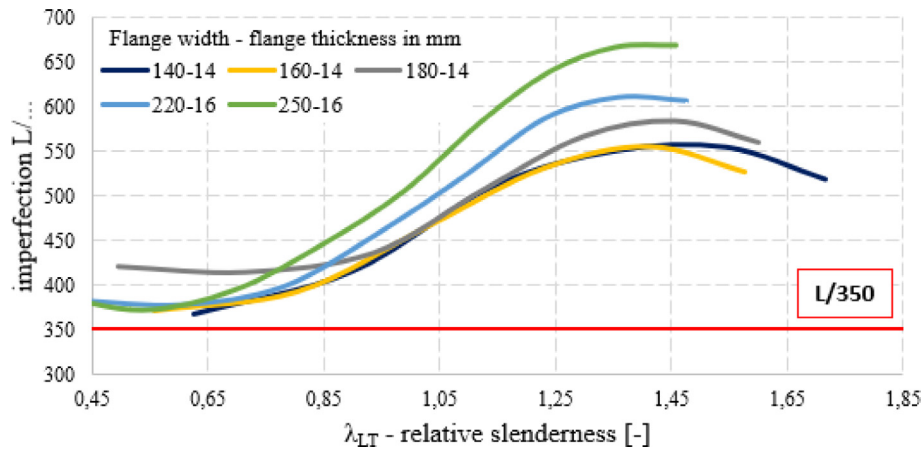
Fig. 7. Scaling factors on *L* of the equivalent geometric imperfection magnitudes in the function of the relative slenderness.

have. The L/1000 is defined by the EN 1090-2 [1] as the largest tolerated value for member out-of-straightness and the residual stress pattern is taken from [27], which model has test-based origin. Therefore, the FEM-based resistances calculated are surly on the safe side. For each type of girder, the load bearing capacities are determined by applying different equivalent geometric imperfection magnitudes and the required equivalent geometric imperfection magnitude is derived by linear interpolation.

Fig. 7 presents the results of the study where the vertical axis represents the scaling factor on the span length *L* and the horizontal axis represents the relative slenderness regarding lateral–torsional buckling according to Eq. (8). M_{cr} is determined by LBA and M_y is the cross-sectional moment capacity calculated by neglecting the web contribution and by considering only the Steiner's terms as a simplification given by Eq. (9) according to EN 1993-1-5 [32] where $b_{\mathrm{f,eff}}$ is the effective width according to Jáger et al. [33,34].

Fig. 7 shows curves representing the equivalence of the impact of equivalent geometric imperfections and initial geometric imperfections combined with residual stresses. One can see that the trend of the curves is the same for all cross-sections. It is shown that the wider the flanges, the smaller is the equivalent geometric imperfection magnitude replacing the effect of residual stresses and out-of-straightness of L/1000. It is also shown that for relative slenderness less than 0.7 the differences are much smaller between the curves while at larger relative slenderness the differences are larger. The study also showed that the change in the corrugation angle had a minor effect; there is no significant difference between the results.

The results suggest that the equivalent geometric imperfection is relative slenderness dependent governed by the varying influence of residual stresses. As a simplification, a constant value of *L*/350 for equivalent geometric imperfection magnitude is proposed to be on the safe side for all geometries and slenderness ranges analyzed.

5. Numerical parametric study

5.1. Effect of the corrugated web layout

The corrugated web periodically varies along the beam length and it influences the stress distributions in the flanges as well proved by [35–37]. It is also proved that the boundary conditions and the support and loading positions compared to the corrugated web have notable effect on the stress distributions [38]. Therefore, different layouts are studied presented in Fig. 8. Six different cases are investigated: axially- (a, b, c, d) or point-symmetrical (e, f) to the midspan having supports at the inclined or parallel fold. For axially symmetric girders two versions of these girders are studied as shown by Fig. 8 (*a, b* and *c, d* in pairs). The difference was the direction of imperfection relative to the corrugation.
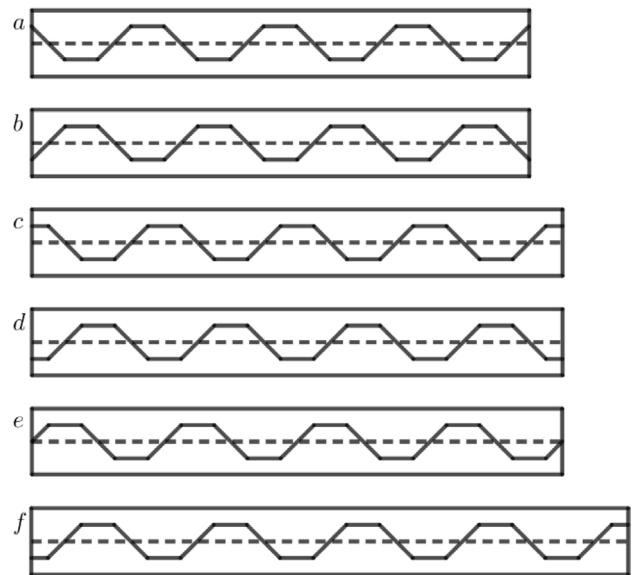

Fig. 8. Studied different corrugated web layouts.

Figs. 9 and 10 show the elastic critical moment and the lateral–torsional buckling resistance, respectively, as a function of span length for different layouts. It can be seen that the layout of the web has no significant influence on either the elastic critical moment or the lateral–torsional buckling resistance of the girders. In both deterministic and stochastic study point-symmetrical girders with starting inclined folds are investigated (*e* in Fig. 8).

5.2. Effect of boundary conditions

Three types of support conditions are applied in the current parametric study:

support #1: fork-type support where the transverse rotation and warping of the end cross-sections are allowed ($k = 1.0$ and $k_{\mathrm{w}} = 1.0$),

support #2: fork-type support with rigid transverse stiffeners anchoring the bimoment ($k = 1.0$ and $k_{\mathrm{w}} = 0.5$),

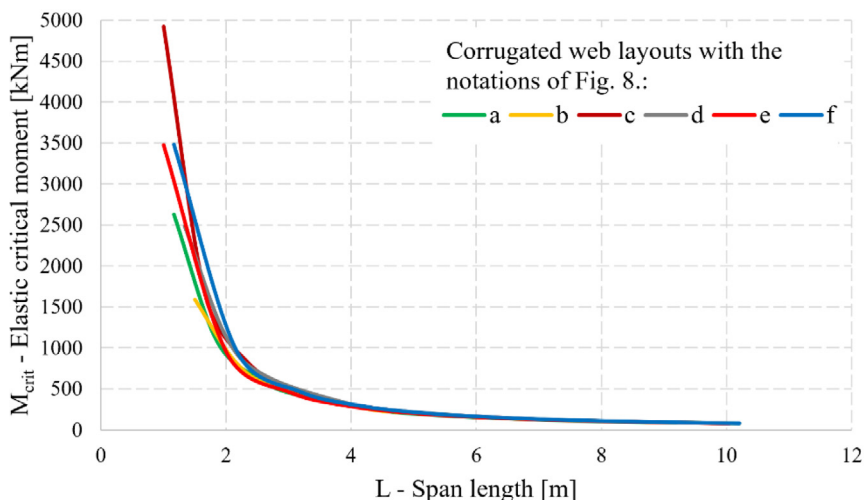**support #3:** transverse rotation and warping are restrained anchoring both the transverse bending moment and bimoment ($k = 0.5$ and $k_{\mathrm{w}} = 0.5$).

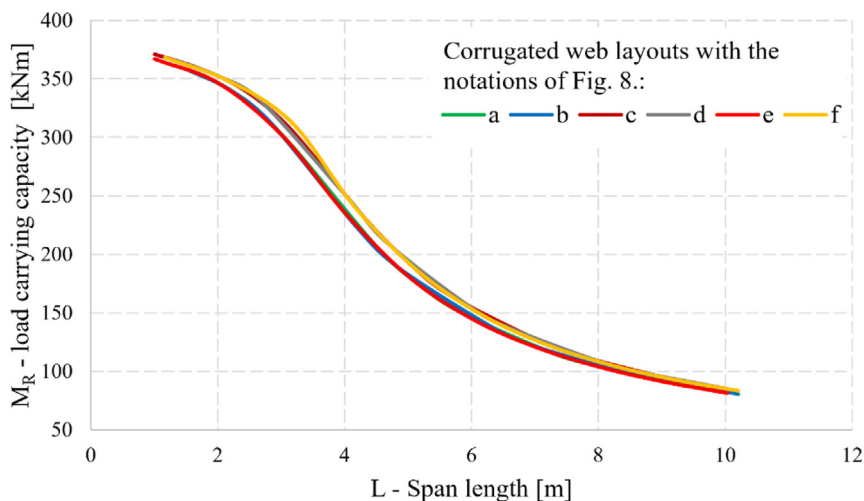**Fig. 9.** Elastic critical moment of girders with different web.

Fig. 10. Lateral–torsional buckling resistance of girders with different web.

5.2.1. Elastic critical moment

The effect of support conditions on the elastic critical moment is shown in Fig. 11., where the vertical and horizontal axes represent the elastic critical moment and the span length L, respectively. The elastic critical moment is calculated in three ways: by linear buckling analysis and with the proposals of Lindner [4] and Lopes et al. [13]. The results show that always the support #1 condition has the lowest elastic critical moment, and the support #3 has the highest elastic critical moment of the girders as it is expected from Eq. (1). It is to be noted that the larger is the span length, the smaller is the influence of the warping term. The support #1 and #2 layouts approach faster and result in the same M_{cr} for large spans where the torsional constant fully governs, and the warping term vanishes. In addition, the differences between the three calculation methods are not spectacular, so it can be seen that the analytical methods approximate the numerical calculations well.

Table 2 collects the statistical evaluation of the differences between the numerical results and analytical proposals. The statistics show that Lindner's approximation is quite accurate for support #1. For the shortest span length, relatively large deviations are found when practically the failure is governed by the strength of material. It is confirmed by the LBA results, since the combination of lateral–torsional and local flange buckling type eigenmode shapes are appeared for short span.

5.2.2. Lateral–torsional buckling resistance

The effect of support conditions on the FEM-based lateral–torsional buckling resistance is shown in Fig. 12. As expected, support #1 has the lowest load carrying capacity where the end cross-sections of the girder are free to rotate and warp, and support #3 has the highest where the end cross-sections are fixed to rotate and warp. It can be also seen that by increasing the span length support type #2 tends faster to support type #1 due to the progressive decreasing influence of the point-like rigid transverse stiffeners meant to anchor the bimoment.

Fig. 13 shows a typical comparative stress diagram (von Mises stress) for each boundary condition for short and long spans. Furthermore, a top view figure illustrates the failure mode shape in all three cases. It can be seen that essentially strength failure occurs for short girders, and LTB for longer girders.

In Fig. 14 all the results are plotted in the relation of the relative slenderness and the reduction factor. The reduction factors are obtained by Eq. (10) where $M_{b,R}$ is the FEM based lateral–torsional buckling resistance for $L/1000$ equivalent geometric imperfection and M_y is the cross-sectional bending moment resistance according to Eq. (9). It can be seen that all the points fall on the same curve regardless of the support conditions with minimal deviations. Therefore, only support type #1 is applied in further numerical simulations.

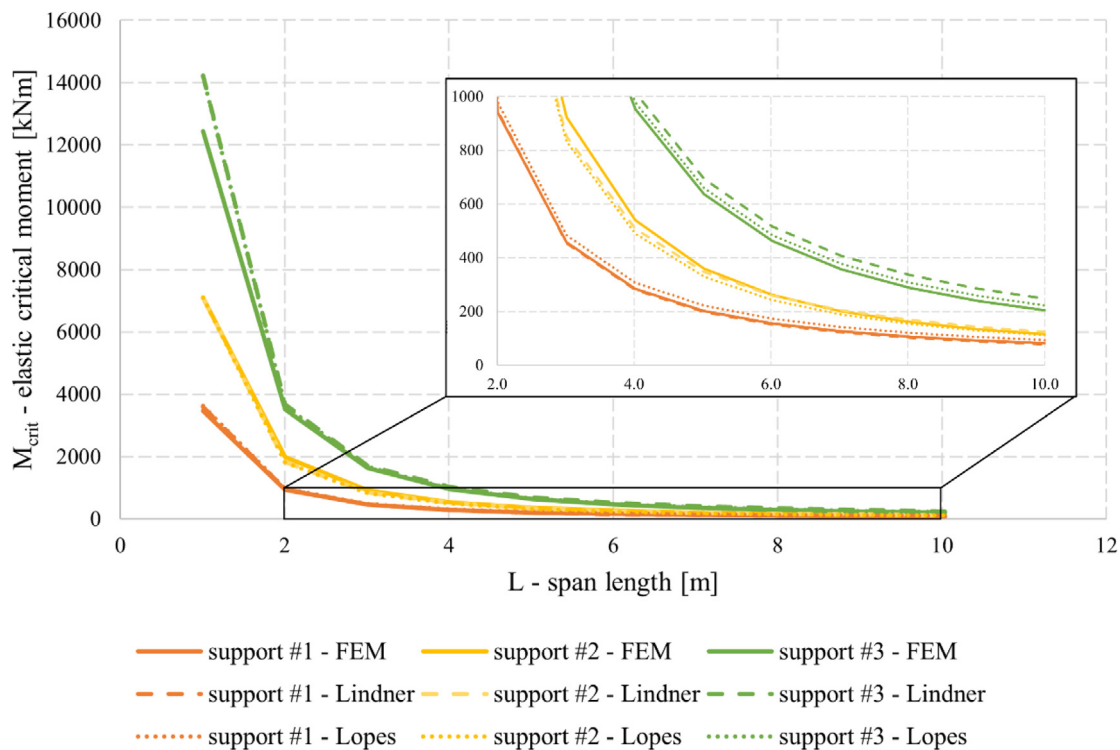$$\chi_{LT} = \frac{M_{b,R}}{M_y} \tag{10}$$

Fig. 11. The effect of support conditions on the elastic critical moment.

Table 2
Comparison of the LBA results and the proposals from literature.

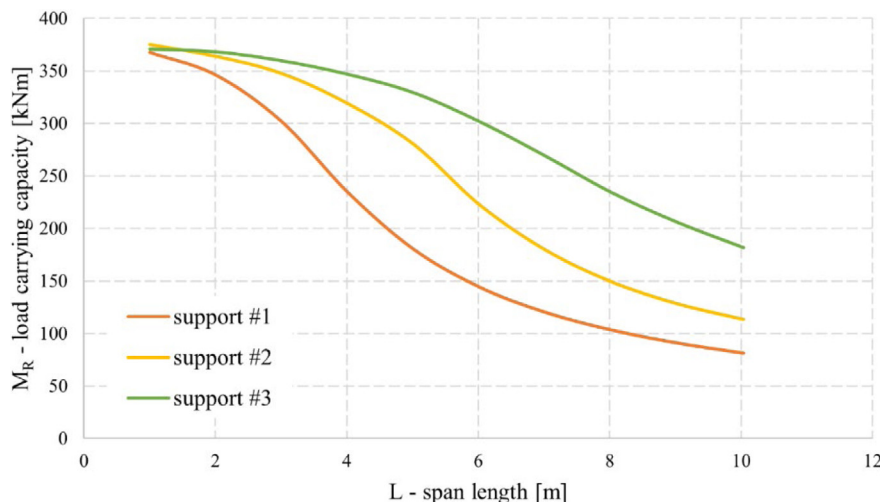|	Support #1		Support #2		Support #3	
	$M_{cr,FEM}/M_{cr,Lindner}$	$M_{cr,FEM}/M_{cr,Lopes}$	$M_{cr,FEM}/M_{cr,Lindner}$	$M_{cr,FEM}/M_{cr,Lopes}$	$M_{cr,FEM}/M_{cr,Lindner}$	$M_{cr,FEM}/M_{cr,Lopes}$
Average	1016	0,911	1009	1066	0,894	0,945
Std. Dev.	0,021	0,032	0,055	0,034	0,045	0,030
CoV	0,021	0,035	0,054	0,032	0,051	0,032
Min	0,964	0,871	0,924	1000	0,825	0,877
Max	1037	0,961	1085	1109	0,959	0,978

Fig. 12. Effect of supports conditions on the load carrying capacity.

5.3. Effect of the steel grade

The use of high-strength steel (HSS - S420 and higher up to S960) in structural engineering practice is increasing rapidly due to the advantages of HSS material. For this reason, in addition to the investigation of normal-strength steels (NSS) high-strength steel is also used in this paper. One girder geometry is studied (140-14 mm flange size, corrugation angle is 45°), the only difference is in the steel material grades, namely: S235, S275, S355, S460 and S960. The material behavior of high-strength steel is different from that of normal-strength steel. The
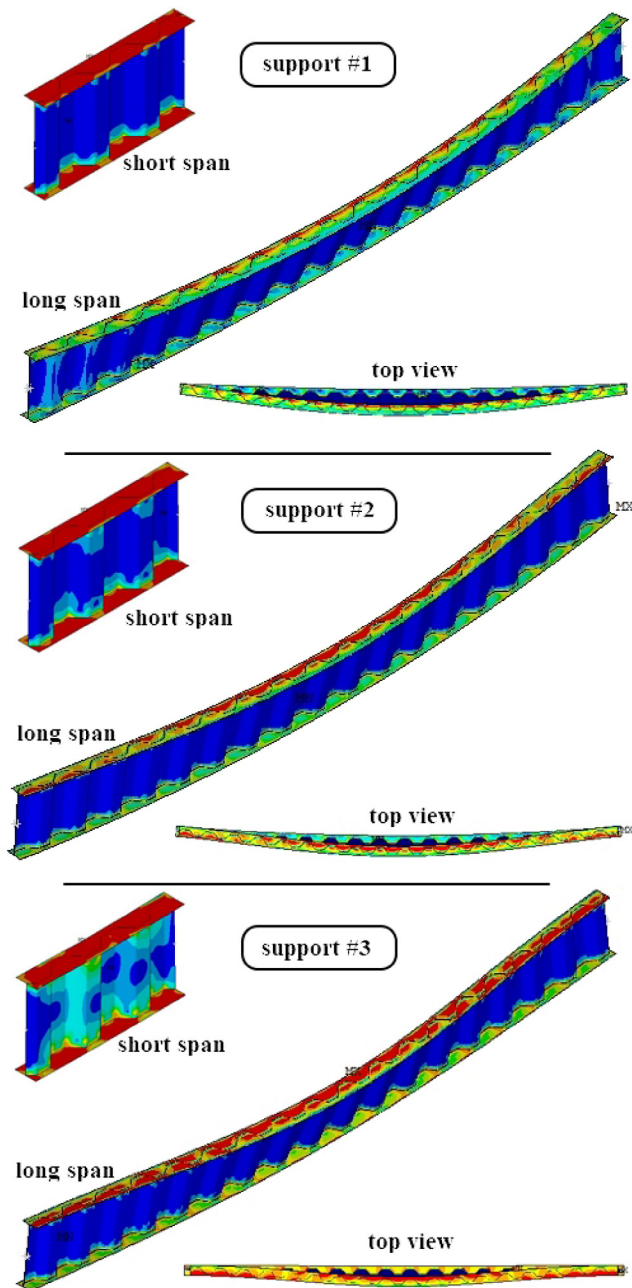
Fig. 13. The typical failure mode of each boundary condition for short and long span.

	f_y [Mpa]	f_u [Mpa]	Material model
S235	235	360	Gardner's
S275	275	430	Gardner's
S355	355	510	Gardner's
S460	460	460 ∗ 1.1	Ramberg–Osgood
S960	960	960 ∗ 1.1	Ramberg–Osgood

based resistance (with L/1000 + residual stresses) and span length, respectively. It is to be noted that for HSS plates the corresponding residual stress pattern is applied according to [40]. It can be seen as the span length increases, the differences in the load bearing capacities are decreasing. It suggests that for high slenderness the steel grade has minor effect on the LTB resistance, which shows elastic buckling of the specimens.

5.3.2. Hybrid girders

Using the combination of two different steel grades two hybrid girder types are investigated:

(i) the web is made of S235 and the flanges are made of S460,
(ii) the web is made of S355 and the flanges are made of S960.

For comparison the reference girders are made of pure S460 or pure S960 steel grades. The results show that the differences are less than 2.5%; meaning that the "accordion effect" is valid for hybrid girders as well when member type buckling governs the failure.

In addition, the results of girders made of pure S355 is compared with the results of girders made of S355 web and S960 flanges in Fig. 17. It is shown that for small relative slenderness the hybrid girders have slightly greater capacity, on the other side for higher relative slenderness ($\lambda_{LT} > 1.0$) the capacity curves, however, coincides. The difference can be explained by the smaller residual stresses in HSS structures. The same tendencies are observed by Somodi and Kövesdi [40] in the case of flexural buckling where curve *a* can be used instead of the buckling curve *b* for HSS columns. This needs further investigations in the future.

6. Deterministic analysis with reliability assessment

6.1. Nonlinear imperfect analysis

Five different cross-sections are investigated in the deterministic study, differing in their flange dimensions and corrugation profile. In all cases, the web height of the girders is 520 mm and the web thickness is 6 mm. The cross-sections are doubly symmetrical; the five types of flanges are 140-14, 160-14, 180-14, 220-16, 250-16 (flange width–flange thickness in mm). For the girders with 140-14 flange, three types of corrugation profile are tested, the only difference being in the corrugation angle: in addition to the traditional 45°, 30° and 40° are also tested, the other parameters are: $a_1 = a_2 = 98$ mm; notations are given in Fig. 1. These girders are studied in 9 to 10 different lengths and the results are plotted in relation with the relative slenderness-reduction factor diagram. The support type #1 is used for the end cross-sections (defined in Section 5.2), the initial geometrical imperfection magnitude is considered by L/1000 out-of-plane straightness and residual stresses are also taken into account.

The elastic critical moments are determined by LBA to calculate the relative slenderness according to Eq. (8). The lateral–torsional buckling resistances are determined by GMNIA, and the reduction factors are derived according to Eq. (10). The results of the deterministic study are compared with EN 1993-1-1 flexural buckling curves (a_0, *a*, *b*, *c*, *d*) are shown in Fig. 18. It can be seen the calculation results lie between the flexural torsional buckling curve *a* and *b*.

The elastic critical moments and thus the relative slenderness are also calculated with the analytical proposals of Lindner and Lopes et al.;
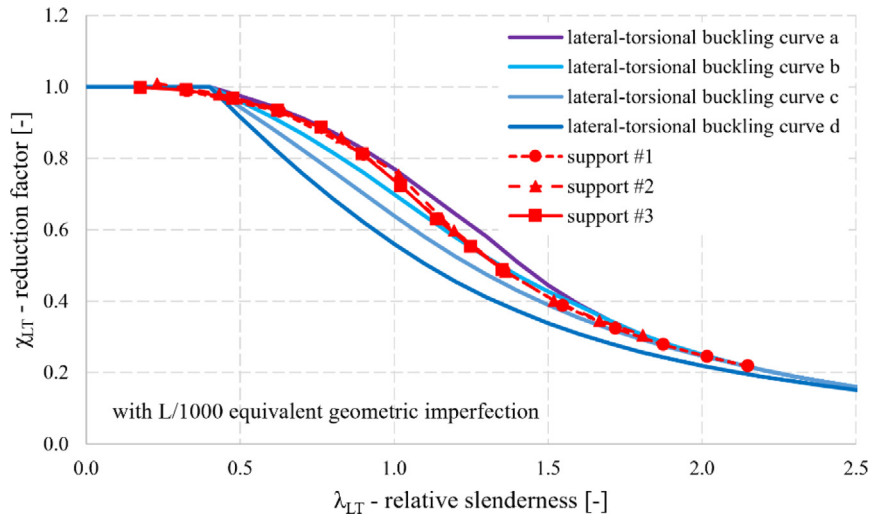
most important differences beside the increased strength are in the ductility and in the hardening phase. For NSS material the Gardner model is used as mentioned earlier, but in the numerical simulations of HSS Ramberg–Osgood-type material model is applied, which is a nonlinear elastic–plastic material model using strain hardening to simulate the behavior of HSS material accurately. The Ramberg–Osgood stress–strain curve is shown in Fig. 15.

The applied steel grades, and their properties is summarized in Table 3.

Throughout this study, the factor $n = 14$ is used to the Ramberg–Osgood equation [39]. This factor was determined by different coupon tests on similar material tests that were available to the authors.

5.3.1. Lateral–torsional buckling resistance

The obtained results regarding the buckling resistance are plotted in Fig. 16 where the vertical and horizontal axes represent the FEM

Fig. 14. Effect of support conditions on the reduction factor.

Table 4
Comparison of the numerical results and proposals using a, b flexural buckling curves and c, d lateral–torsional buckling curves of EN1993-1-1.

|	λ_{LT} from $M_{cr,FEM}$ and from $M_{cr,Lindner}$				λ_{LT} from $M_{cr,FEM}$ and $M_{cr,Lopes}$			
	$\chi_{a.FEM}/\chi_{a.Lindner}$	$\chi_{b.FEM}/\chi_{b.Lindner}$	$\chi_{c.FEM}/\chi_{c.Lindner}$	$\chi_{d.FEM}/\chi_{d.Lindner}$	$\chi_{a.FEM}/\chi_{a.Lopes}$	$\chi_{b.FEM}/\chi_{b.Lopes}$	$\chi_{c.FEM}/\chi_{c.Lopes}$	$\chi_{d.FEM}/\chi_{d.Lopes}$
Average	1.007	1.006	1.007	1.006	0.994	0.993	0.995	0.995
Std. Dev.	0.011	0.030	0.011	0.010	0.032	0.038	0.029	0.027
CoV.	0.011	0.030	0.010	0.010	0.032	0.038	0.029	0.027
Min.	0.996	0.954	0.995	0.992	0.881	0.905	0.881	0.896
Max.	1.036	1.058	1.038	1.031	1.031	1.056	1.027	1.026
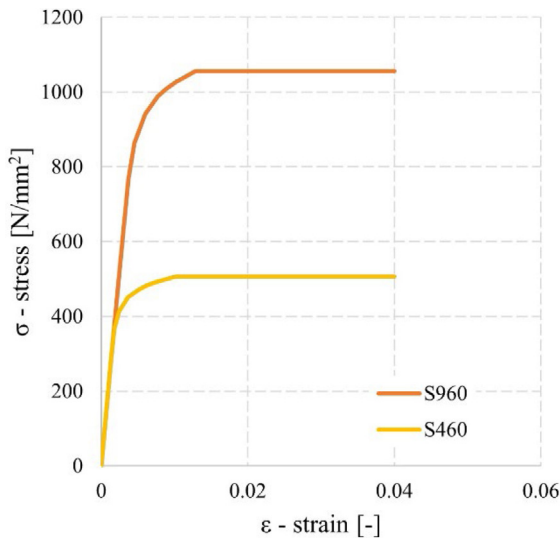
Fig. 15. Ramberg–Osgood stress–strain curve (used for HSS).

results are shown in Fig. 19. The three different colors of the points in the figure represent the three different ways of determining the relative slenderness. Table 4 presents the comparison of the reduction factors from the numerically obtained relative slenderness and from *a* and *b* flexural buckling and *c* and *d* lateral–torsional curves using the relative slenderness derived from the elastic critical moments of Lindner and Lopes et al.

It can be seen that Lindner's proposal fits the numerical results slightly better than Lopes' equation; and Lindner's proposal results in slightly higher resistances. There are negligible differences in the average of the ratio of the corresponding reduction factors, in both

cases (less than 1%), but the differences in standard deviation are larger for Lopes' proposal. The results show that Lindner's proposal is more on the safe side.

6.2. Partial factor γ_{M1} determination

In the statistical evaluation the results are compared with the lateral–torsional buckling curves *c* and *d* ($\beta = 0.75$ and $\lambda LT,0 = 0.4$) and with the flexural buckling curves *a* and *b* of EN1993-1-1 [2]. A comparison of the four curves with the LBA and GMNIA results is shown in Fig. 20.

Using statistical evaluation, the safety levels of the proposed buckling curves are determined in order to obtain the required partial safety factor (γ_{M1}). The calculation of the necessary statistical parameters is executed based on the prescriptions of the EN 1990 Annex D [3]. The applied method is summarized in Eqs. (11)–(22). The expected value of the correction factor (*b*) can be calculated by comparing the FEM based resistances ($r_{e,i}$) and the theoretical values ($r_{t,i}$). It may be estimated by the least squares' method according to Eq. (11).

$$b = \frac{\sum r_{e,i} \cdot r_{t,i}}{\sum r_{t,i}^2} \tag{11}$$

The error term can be calculated for each numerical calculation by Eq. (12).

$$\delta_i = \frac{r_{e,i}}{b \cdot r_{t,i}} \tag{12}$$

The coefficient of variation of the error term (V_δ) can be estimated by Eqs. (13)–(16) where *n* is the number of the sample.

$$V_\delta = \sqrt{e^{(s_\Delta^2)} - 1} \tag{13}$$

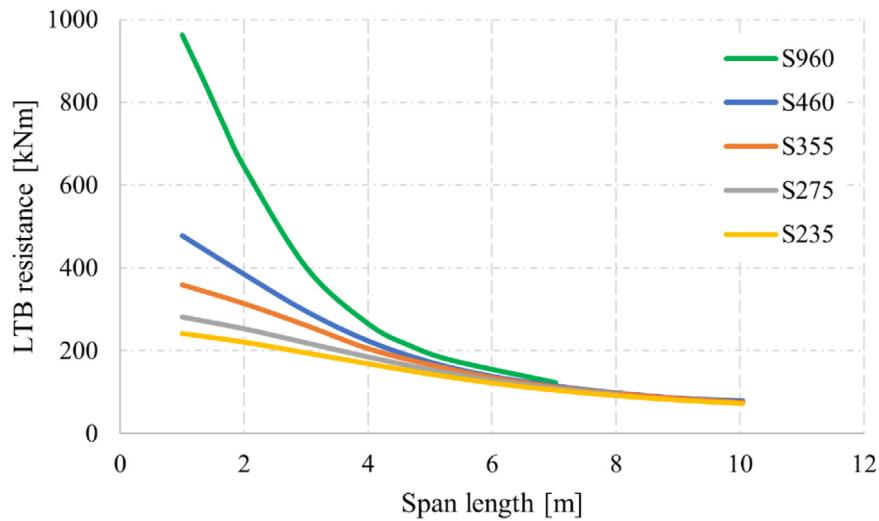$$s_\Delta^2 = \frac{1}{n-1} \sum_{i=1}^{n} (\Delta_i - \overline{\Delta})^2 \tag{14}$$

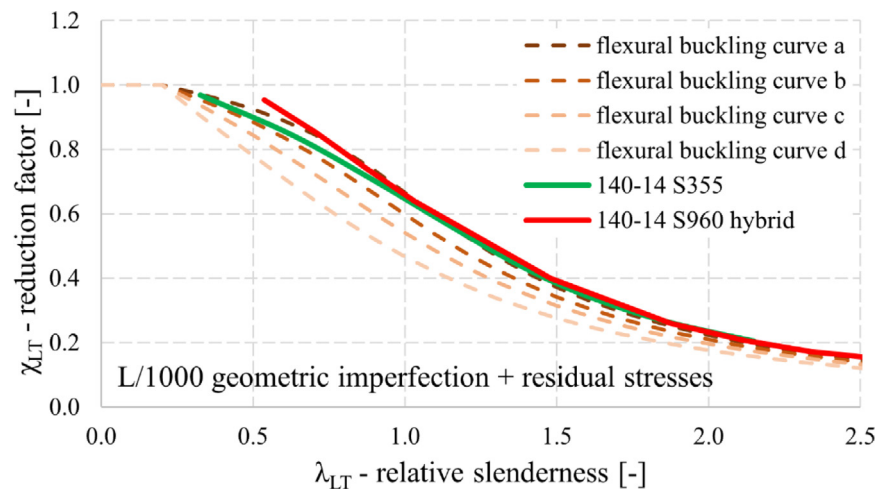**Fig. 16.** Effect of the steel grade on LTB resistance.

Fig. 17. Comparison of the results of the pure S355 and the S960–S355 hybrid girders with the buckling curves of EN1993-1-1 [2].
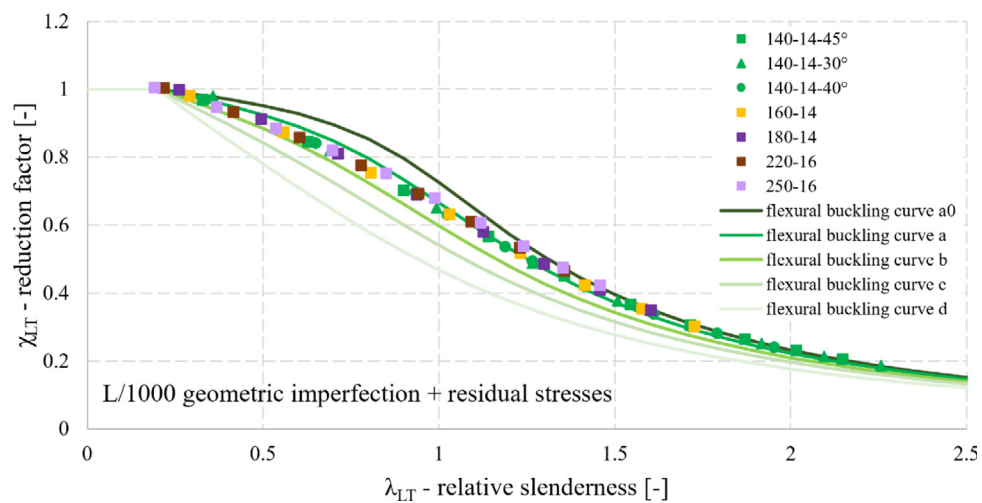

Fig. 18. Comparison of the LBA and GMNIA results of the deterministic analysis with EN 1993-1-1 flexural buckling curves.

$$\overline{\Delta} = \frac{1}{n} \sum_{i=1}^{n} \Delta_i \tag{15}$$

$$\Delta_i = \ln(\delta_i) \tag{16}$$

EN 1990 Annex D also specifies how to determine the characteristic value of the resistance from the test results. If a large number of experimental results are available Eqs. (17)–(18) can be applied where
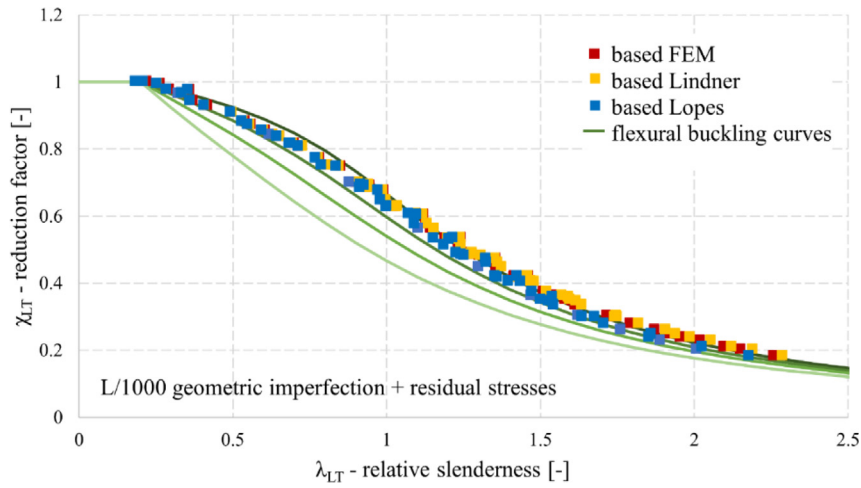
Fig. 19. Comparison of the results of the deterministic analysis with EN 1993-1-1 flexural buckling curves. (For interpretation of the references to color in this figure legend, the reader is referred to the web version of this article.)
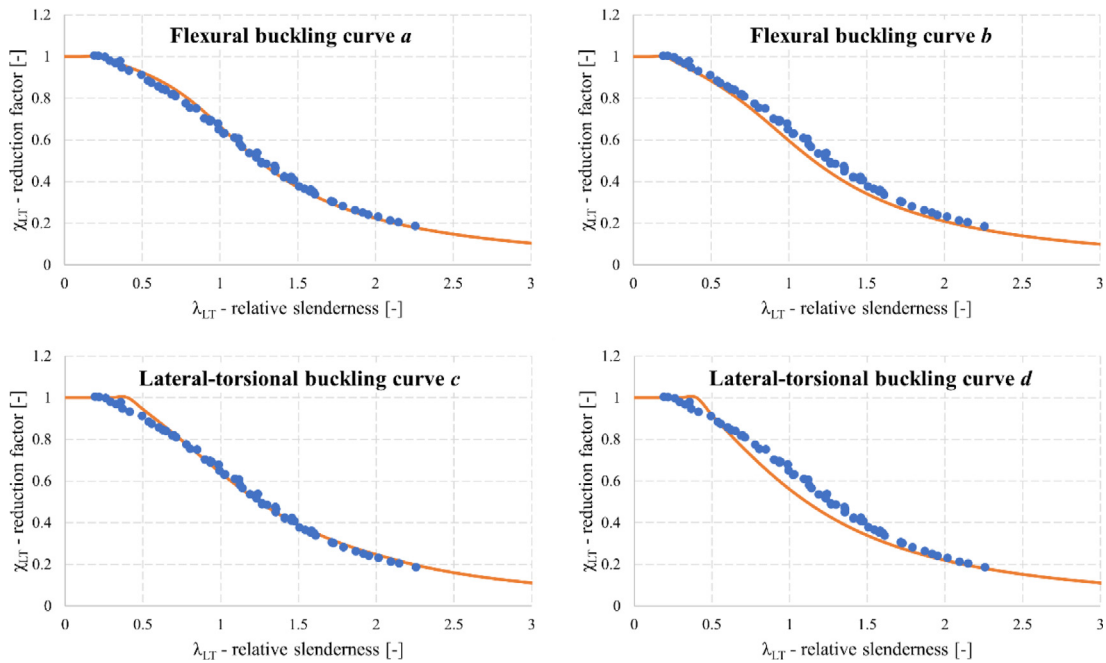

Fig. 20. The results of the deterministic analysis and the flexural buckling curves *a*, *b* and lateral–torsional buckling curves *c*, *d* of EN1993-1-1.

$g_{rt}(X_m)$ is the theoretical resistance calculated from the resistance function, $k_\infty = 1.64$ is the characteristic value defined as the lower 5% quantile of the experimental resistances, since $\phi(1.64) = 1/19.8 = 5.05\%$; namely one out of 20 structural elements can have a resistance lower than the characteristic resistance.

$$r_k = b \cdot g_{rt}(X_m) \exp(-k_\infty \cdot Q - 0.5 \cdot Q^2) \tag{17}$$

$$Q = \sqrt{\ln(V_r^2 + 1)} \tag{18}$$

The coefficient of variation V_r is composed of V_δ and V_{xi}, if they are small and can be calculated by Eq. (19).

$$V_r^2 = (V_\delta^2 + 1) \cdot \left[\prod_{j=1}^{n} (V_{Xi}^2 + 1) \right] - 1 \tag{19}$$

The coefficients of variation of design variables can only be calculated from experimental results if the test population is fully representative of the variations that occur. In reality, they can be taken from previous

research results as prior data. Based on the recommendations of JCSS (Joint Committee on Structural Safety) [41] for the plate thickness $V_t = 0.05$ and for the plate width $V_b = 0.005$ are applied. The partial factor determination can be done by Eqs. (20)–(22) where $Q_{fy} = 0.07$ is considered according to JCSS [41].

$$\gamma_M^* = \Delta k \cdot \gamma_M \tag{20}$$

$$\gamma_M = \frac{r_k}{r_d} = \exp(1.4 \cdot Q) \tag{21}$$

$$\Delta k = \frac{\exp(-2Q_{fy} - 0.5Q_{fy}^2)}{b \cdot \exp(-k_\infty Q - 0.5Q^2)} = \frac{0.867}{b \cdot \exp(-1.64 \cdot Q - 0.5 \cdot Q^2)} \tag{22}$$

The resulting γ_{M1} partial factors are summarized in Table 5. The smallest γ_{M1} partial factor belongs to the flexural buckling curve *b*, but for each investigated flexural buckling and lateral–torsional buckling curves the values are in between 1.0 and 1.1.
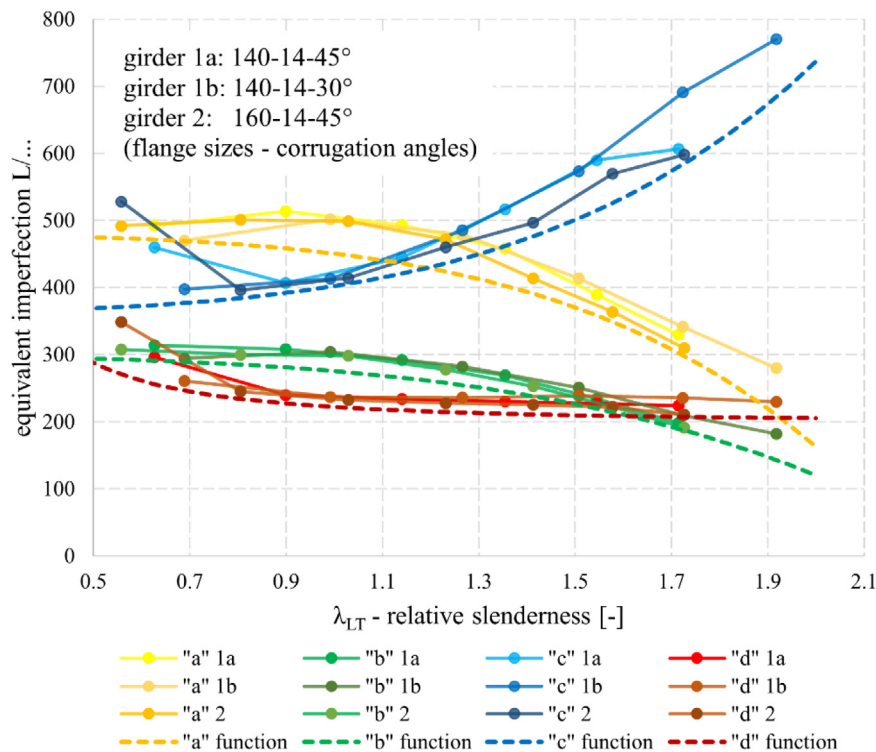
Fig. 21. Equivalent geometrical imperfections required to recover the load capacity values corresponding to the standard buckling curves *a* and *b* and lateral–torsional buckling curves *c* and *d* as a function of relative slenderness and their approximation functions. (For interpretation of the references to color in this figure legend, the reader is referred to the web version of this article.)

Table 5
Partial factors γ_{M1} obtained from the deterministic nonlinear analysis.

	γ_{M1}
a flexural buckling curve	1.05619
b flexural buckling curve	1.01618
c lateral–torsional buckling curve	1.05622
d lateral–torsional buckling curve	1.07525

Table 6
Relative slenderness dependent required equivalent geometric imperfection magnitudes assigned to buckling curves.

Buckling curve	Scaling factors for equivalent geometric imperfection magnitude $[L/\ldots]$
a flexural	$480 - (\lambda_{LT} + 0.85)^{5.5}$
b flexural	$300 - (\lambda_{LT} + 0.95)^{4.8}$
c lateral–torsional	$360 + (\lambda_{LT} + 1)^{5.4}$
d lateral–torsional	$200 + \frac{22}{\lambda_{LT}^2}$

6.3. Required equivalent geometrical imperfections for each buckling curves

The results of the deterministic nonlinear analysis are used to determine the required relative slenderness dependent equivalent geometric imperfection magnitudes to recover the FEM-based resistance assigned to the flexural and lateral–torsional buckling curves of the EN1993-1-1. Three girder geometries are studied where the flange sizes are 140-14 mm (girder 1) and 160-14 mm (girder 2), the corrugation angles are set to $\alpha = 30°$ (angle *a*) and $\alpha = 45°$ (angle *b*), and the web fold lengths are set $a_1 = a_2 = 98$ mm. Within the numerical parametric study, the magnitude of the equivalent geometric imperfection is changed and the buckling resistance is determined. To each analyzed girder geometry the necessary equivalent geometric imperfection magnitude is determined to get equivalent buckling resistance obtained by buckling curves of the EN 1993-1-1 [2]. Results of the parametric study is shown in Fig. 21. The horizontal axis presents the relative slenderness of the girders and the vertical axis shows the necessary equivalent geometric imperfection magnitude.

In the investigated parameter domain the results prove that there are no significant differences coming from the geometric variation. In Fig. 21 the results are plotted with four different colors according to the four different buckling curves. It can be seen that three curves with the same color show a good agreement. For the four buckling curves four approximate functions are plotted which depend only on the relative slenderness. Table 6 gives these functions represented

by the dashed lines in Fig. 21. In other words, by these functions the equivalent geometric imperfection magnitudes – using the global buckling eigenmodes – can be determined in order to reproduce FEM-based resistance results which lie on the given buckling curve with a small scatter.

7. Stochastic analysis with reliability assessment

Stochastic numerical analysis is executed for trapezoidally corrugated web girders. Numerous Monte Carlo simulations are executed, and the lower 5% quantile value of the FEM-based lateral–torsional buckling resistance is determined in relation with the relative slenderness. In stochastic numerical analysis, three different girders are investigated: (i) the basic case when the girder has 140-14 mm flanges and corrugation angle of $\alpha = 45°$, (ii) a different cross-section (160-14 mm flange, $\alpha = 45°$) and (iii) a different corrugation angle (160-14 mm flange, $\alpha = 30°$). The other parameters of corrugation profile do not change: $a_1 = a_2 = 98$ mm, $a_3 = a_4 = 69$ mm. The steel grade of S355 is applied in each simulation. Six different relative slenderness cases of each girder geometries are performed and in overall $3 \times 6 \times 30 = 540$ independent Monte Carlo simulations are carried out.
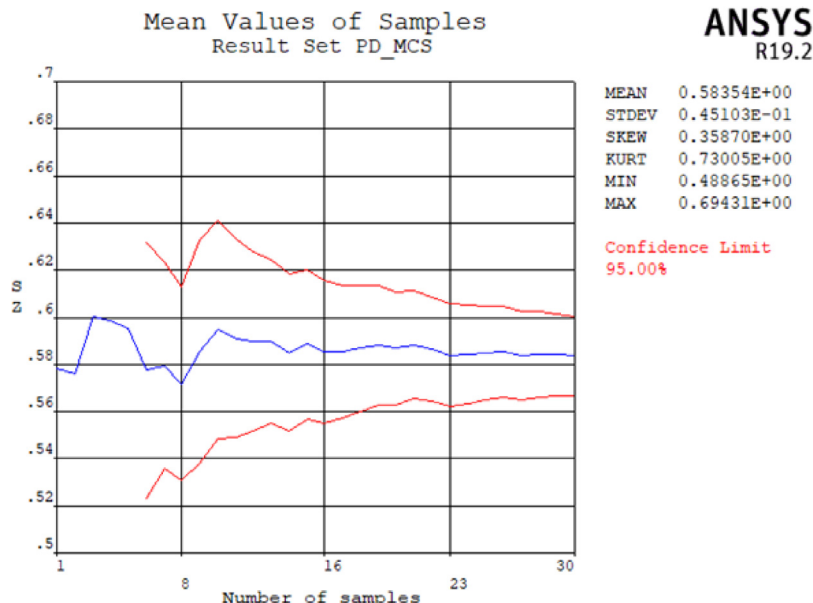
Fig. 22. Change in the average lateral–torsional buckling resistance over 30 experiments.

Table 7
Properties of the probabilistic variables.

Variable		Distribution type	Mean value	CoV
Yield strength	f_y	Lognormal	Nominal/0.8892	0.07
Web height	h_w	Normal	Nominal	0.005
Web thickness	t_w	Normal	Nominal	0.05
Flange width	b_f	Normal	Nominal	0.005
Flange thickness	t_f	Normal	Nominal	0.05

7.1. Variables of the probabilistic analysis

In the stochastic analysis five parameters are treated as probabilistic variable with a certain distribution type, mean value and coefficient of variation summarized in Table 7. Normal distribution is defined for the geometrical parameters according to the recommendation of JCSS [41]. Based on this recommendation the coefficient of variation (CoV) is set equal to $V_t = 0.05$ for each thickness and $v_b = 0.005$ for each plate width. The mean value is assumed to be equal by the nominal value for the geometrical parameters. According to JCSS [41] the distribution of the yield strength has lognormal distribution with a coefficient of variation of $V_{fy} = 0.07$. According to EN 1993-1-1 [2] the nominal value of a steel grade should be treated as the characteristic value of the yield strength. According to EN 1990 [3] the characteristic value should be defined as the 5% quantile value. In case of lognormal distribution and $V_{fy} = 0.07$ the 5% quantile equals to 0.8892 ($1 - 1.583 \times 0.07$) times the mean value. Therefore, the mean value is calculated from the nominal value of the steel grade according to Eq. (23). In the stochastic numerical analysis, the geometrical imperfection magnitude is not a probabilistic variable, it is always set to $L/1000$; it is also valid for the residual stress pattern.

$$f_{y,m} = \frac{f_{y,nom}}{0.8892} \tag{23}$$

7.2. Details of the stochastic numerical analysis

In the stochastic analysis the Latin Hypercube Sampling (LHS) is used which has the special feature of selecting values at the limits of the distribution with low probability. This is of great importance in this case, since the objective is to determine the characteristic resistance to

turning out for which the lower 5% quantile must be determined. It is also advantageous that the LHS avoids clustering of selected values during random generation whereas in the conventional Monte Carlo method it is often the case for small samples that points are clustered close together in some ranges while other ranges remain empty.

The number of samples (n) required for a Monte Carlo simulation depends on the probability sought. For the evaluation of low probability ranges if P is the probability sought, a minimum sample size of n from $30/P$ to $100/P$ is needed for a reliable result. For the characteristic resistance ($P = 5\%$) $n \approx 600–2000$ specimens should be tested. It is advisable to reduce the number of samples. This is possible with the response surface method where a response surface is fitted to the Monte Carlo simulation results using different regression models. The runs use a quadratic (second order) regression model according to Eq. (24) where x is the vector of the variables, A is the quadratic coefficient matrix, k is the linear coefficient matrix and m is a constant.

$$RespSurf = \overline{x} \cdot \overline{\overline{A}} \cdot \overline{x}^T + \overline{k} \cdot \overline{x}^T + m \tag{24}$$

The number of probability variables determines how many samples are needed in the Monte Carlo simulation to fit the response surface correctly. In the stochastic analysis five probability variables are used in which there are 21 coefficients in the second-degree polynomial, and a minimum of 27 samples (points) are needed to produce [28].

When running a new Monte Carlo simulation on the matched response surface, the load capacities are not determined by new runs, but by using the approximation function created for the response surfaces which made the calculation of the results much faster. Thus, in the first step $n_1 = 27$ (or more) and in the second step $n_2 = 100000$ buckling resistances are obtained, giving the sample number needed for the evaluation.

7.3. Results of the stochastic nonlinear analysis

From the executed 540 independent Monte Carlo simulations one is chosen to present the applied evaluation method and the obtained results in a detailed manner. Fig. 22 shows how the average of the load capacities varies during the execution of $n_1 = 30$ experiments. It is clear from the graph that the 27 samples required are sufficient for further calculations, as the curve flattens out and the average is practically unchanged for the last 10 experiments.
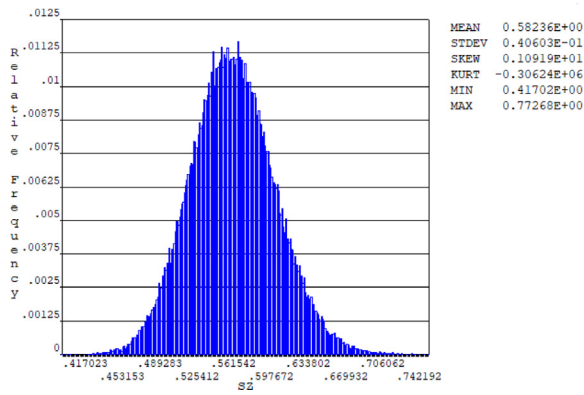
Fig. 23. Histogram of the resulting lateral–torsional buckling resistance.

the flexural buckling curve *b* of EN1993-1-1 can be used safely using $\gamma_{M1} = 1.0$ with imperfections given in Section 3.

8. Conclusions

In the present paper a numerical parametric study is performed by deterministic and stochastic nonlinear imperfect analyses to determine the required equivalent geometrical imperfection and the required buckling curve of EN1993-1-1 for the design of trapezoidally corrugated web girders for lateral torsional buckling. Based on the numerical study the following conclusions are drawn:

- Global eigenmode shape is applied as artificial geometric imperfections. The required equivalent geometric imperfection is determined in such a way to have the same impact on the FEM based resistance as the initial geometric imperfection with magnitude of L/1000 combined with the residual stresses have. A simplified lower bound value of L/350 for equivalent geometric imperfection magnitude is proposed.
- The required equivalent geometric imperfection magnitude is determined for four buckling curves in relation with relative slenderness.
- The corrugated web layout has practically no effect on the elastic critical moment and lateral–torsional buckling resistance for corrugation angles larger than 30°.
- Three different boundary conditions are studied according to the warping and transverse rotation capabilities of the end cross-sections. It is revealed that the proposal of Lindner and Lopes et al. fit well for the elastic critical moment. In addition, the boundary condition has no effect on the buckling resistance.
- Pure normal-strength (NSS), pure high-strength steels (HSS) and hybrid girders are studied. The results show that the flanges govern the LTB resistance of the girders. The use of HSS is advantages for short, unbraced spans while for longer spans the extra material strength vanishes since the buckling governs the failure. In addition, in the inelastic range of the buckling curve the HSS flanges result in slightly greater reduction factors than the NSS flanges having the same relative slenderness.
- The deterministic analysis combined with reliability assessment results show that the flexural buckling curve *b* could be applicable with partial safety factor $\gamma_{M1} = 1.0$.
- The stochastic analysis combined with reliability assessment results confirmed the results obtained from the deterministic analysis.
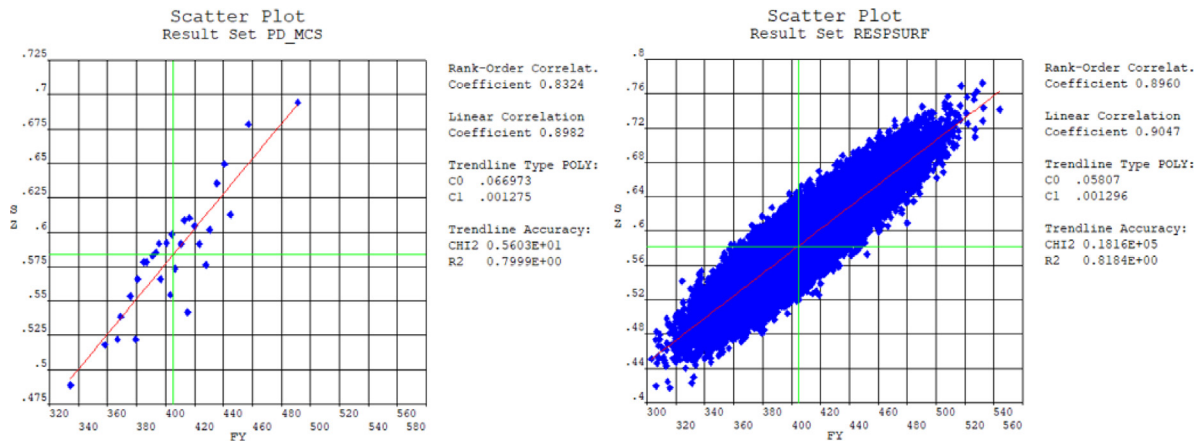
In Fig. 23 the histogram of the load capacities determined in the Monte Carlo simulation shows that the final results follow an approximately normal distribution.

Fig. 24 shows the results of the first 30 Monte Carlo simulations and the 100 000 values obtain by the response surface method as a function of the yield strength. A linear trend line can be fitted to the resulting load capacities and the two figures illustrate the effectiveness of the response surface method. The same diagrams for each probability variable are retrieved in the program.

This calculation has been performed for several slenderness, and for each of them the average value of the load capacities and the characteristic value have been determined. Fig. 25 shows the results with the flexural and lateral–torsional buckling curves of the standard for comparison. It can be seen that the curve obtained for the characteristic values is consistently above the flexural buckling curve *b* and the curve for the mean values is significantly above the flexural buckling curve *a*.

In the statistical evaluation the results are compared with the *b* flexural buckling curve of EN1993-1-1 which fits the best. The partial safety factor (γ_{M1}) is determined as previously presented in the case of the deterministic analysis according to Eqs. (11)–(22). There are two ways to determine γ_{M1} partial safety factor. First, if the ratio of mean value of lower 5% quantile value and the standard deviation is determined for each slenderness, and then average coefficient of variation is calculated; by this γ_{M1} is obtained to 0.981. Second, if the γ_{M1} is determined for each slenderness and then the average γ_{M1} is determined; by this γ_{M1} is obtained to 0.963. It can be seen that

Fig. 24. Yield strength–lateral–torsional buckling resistance diagram from the 30 Monte Carlo simulation (left) and from the response surface method (right).
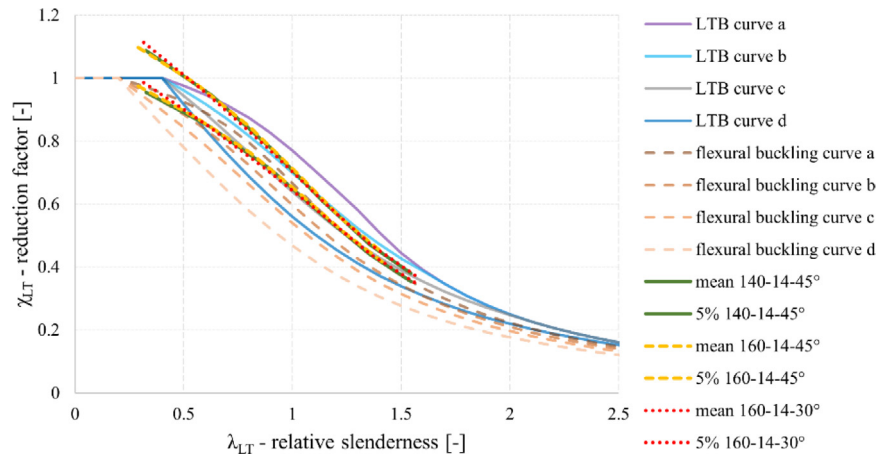
Fig. 25. Comparison of the stochastic analysis results with the buckling curves of EN1993-1-1.

CRediT authorship contribution statement

E. Bärnkopf: Writing – original draft, Software, Investigation. **B. Jáger:** Writing – review & editing, Supervision, Software, Methodology, Conceptualization. **B. Kövesdi:** Writing – review & editing, Supervision, Methodology.

Declaration of competing interest

The authors declare that they have no known competing financial interests or personal relationships that could have appeared to influence the work reported in this paper.

Data availability

The authors do not have permission to share data.

Acknowledgments

References

[1] EN 1090-2:2018, Execution of steel structures and aluminium structures - Part 2: Technical requirements for steel structures.

[2] EN 1993-1-1:2005, Eurocode 3: Design of steel structures - Part 1.1: General rules and rules for buildings.

[3] EN 1990, Eurocode: Basis of structural design.

[4] J. Lindner, Lateral torsional buckling of beams with trapezoidally corrugated webs, in: Proceedings of the 4th International Colloquium on Stability of Steel Structures, Budapest, Hungary, 1990, pp. 79-82.

[5] E.Y. Sayed-Ahmed, Lateral torsion-flexure buckling of corrugated web steel girders, Proc. Inst. Civ. Eng.: Struct. Build. 158 (1) (2005) 53–69.

[6] J. Moon, J. Yi, B.H. Choi, H.E. Lee, Lateral–torsional buckling of I-girder with corrugated webs under uniform bending, Thin-Walled Struct. 47 (2009) 21–30.

[7] N.D. Nguyen, S.N. Kim, S.R. Han, Y.J. Kang, Elastic lateral–torsional buckling strength of I girder with trapezoidal web corrugations using a new warping constant under uniform moment, Eng. Struct. 32 (2010) 2157–2165.

[8] Z. Zhang, G. Li, F. Sun, Flexural–torsional buckling of H-beams with corrugated webs, Adv. Mater. Res. 163–167 (2011) 351–357.

[9] M. Larsson, J. Persson, Lateral–Torsional Buckling of Steel Girders with Trapezoidally Corrugated Webs, Vol. 57 (MSc thesis), Gothenburg, Sweden, 2013.

[10] V. Ilanovsky, Assessment of bending moment resistance of girders with corrugated web, Pollack Period. 10 (2) (2015) 35–44.

[11] S.P. Timoshenko, J.M. Gere, Theory of Elastic Stability, 2nd ed, McGraw-Hill, London, 1961.

[12] S.A. Ibrahim, Lateral torsional buckling strength of unsymmetrical plate girders with corrugated webs, Eng. Struct. 81 (2014) 123–134.

[13] G.C. Lopes, C. Couto, P.V. Real, N. Lopes, Elastic critical moment of beams with sinusoidally corrugated webs, J. Construct. Steel Res. 129 (2017) 185–194.

[14] C. Guo, J. Papangelis, Torsion of beams with corrugated webs, in: Proceedings of the Ninth International Conference on Advances in Steel Structures, Hong Kong, China, 5-7 December, 2018, pp. 373-382.

[15] N.K.H.R. Kazemi, Lateral bracing of I-girder with corrugated webs under uniform bending, J. Construct. Steel Res. 66 (2010) 1502–1509.

[16] J. Moon, N.H. Lim, H.E. Lee, Moment gradient correction factor and inelastic flexural–torsional buckling of I-girders with corrugated steel webs, Thin-Walled Struct. 62 (2013) 18–27.

[17] M.F. Hassanein, A.A. Elkawas, Y.-B. Shao, M. Elchalakani, A.M. El Hadidy, Lateral- torsional buckling behaviour of mono-symmetric S460 corrugated web bridge girders, Thin-Walled Struct. 153 (2020) 106803.

[18] A.A. Elkawas, M.F. Hassanein, M. Elchalakani, Lateral–torsional buckling strength and behaviour of high-strength steel corrugated web girders for bridge construction., Thin-Walled Struct. 122 (2018) 112–123.

[19] Y.-B. Shao, Y.-M. Zhang, M.F. Hassanein, Strength and behaviour of laterally-unrestrained S690 high-strength steel hybrid girders with corrugated webs, Thin-Walled Struct. 150 (2020) 106688.

[20] M.F. Hassanein, A.A. Elkawas, Y.-B. Shao, Assessment of the suitability of eurocode design model for corrugated web girders with slender flanges, Structures 27 (2020) 1551–1569.

[21] M. Kubo, K. Watanabe, Lateral–torsional buckling capacity of steel girders with corrugated web plates, Doboku Gakkai Ronbunshuu A 63 (1) (2007) 179–193.

[22] D. Hannebauer, Zur Querschnitts- Und Stabtragfäigkeit Von TräGern Mit Profilierten Stegen (PhD dissertation), Brandenburgischen Technischen Universität, Cottbus, Germany, 2008.

[23] R.J. Pimenta, G. Queiroz, S.M.C. Diniz, Reliability-based design recommendations for sinusoidal-web beams subjected to lateral–torsional buckling, Eng. Struct. 84 (2015) 195–206.

[24] Z. Zhang, S. Pei, B. Qu, Cantilever welded wide-flange beams with sinusoidal corrugations in webs: Full-scale test and design implications, Eng. Struct. 144 (2017) 163–173.

[25] B. Jáger, B. Kövesdi, L. Dunai, Experimental study on the lateral–torsional buckling strength of trapezoidally corrugated web girders, in: Proceedings of SSRC Annual Stability Conference, St. Louis, Missouri, USA, 2019.

[26] B. Jáger, L. Dunai, B. Kövesdi, Lateral–torsional buckling strength of corrugated web girders - Experimental study, Structures 43 (2022) 1275–1290.

[27] B. Jáger, L. Dunai, 'Nonlinear imperfect analysis of corrugated web beams subjected to lateral–torsional buckling, Eng. Struct. 245 (2021) 112888.

[28] ANSYS® v19.2, Canonsburg, Pennsylvania, USA.

[29] L. Gardner, X. Yun, A. Fieber, L. Macorini, Steel design by advanced analysis: Material modeling and strain limits, Engineering 5 (2019) 243–249.

[30] L. Huang, H. Hikosaka, K. Komine, Simulation of accordion effect in corrugated steel web with concrete flanges, Comput. Struct. 82 (2004) 2061–2069.

[31] S. Mori, T. Miyoshi, H. Katoh, N. Nishimura, S. Nara, A study on local stresses of corrugated steel webs in PC bridges under prestressing, Tech. Memo. Public. Works. Res. Inst. 4009 (2006) 449–458.

[32] EN 1993-1-5:2005, Eurocode 3: Design of steel structures Part 1-5: Plated structural elements.

[33] B. Jáger, L. Dunai, B. Kövesdi, Flange buckling behavior of girders with corrugated web – Part I: Experimental study, Thin-Walled Struct. 118 (2017) 181–195.

[34] B. Jáger, L. Dunai, B. Kövesdi, Flange buckling behavior of girders with corrugated web – Part II: Numerical study and design method development, Thin-Walled Struct. 118 (2017) 238–252.

[35] R. Aschinger, J. Lindner, Zu besonderheiten bei trapezstegtragern, Stahlbau 66 (1997) 136–142.

[36] H.H. Abbas, R. Sauce, R.G. Driver, Simplified analysis of flange transverse bending of corrugated web I-girders under in-plane moment and shear, Eng. Struct. 29 (2007) 2816–2824.

[37] B. Kövesdi, B. Jáger, L. Dunai, Stress distribution in the flanges of girders with corrugated webs, J. Construct. Steel Res. 79 (2012) 204–215.

[38] B. Kövesdi, B. Jáger, L. Dunai, Bending and shear interaction behaviour of girders with trapezoidally corrugated webs, J. Construct. Steel Res. 121 (2016) 383–397.

[39] B. Somodi, B. Kövesdi, Comparison of safety factor evaluation methods for flexural buckling of HSS welded box section columns, Structures 15 (2018) 43–55.

[40] B. Somodi, B. Kövesdi, Flexural buckling resistance of welded HSS box section members, Thin-Walled Struct. 119 (2017) 266–281.

[41] Joint Committee of Structural Safety (JCSS), Probabilistic Model Code, Internet Publication, 2002.